

光电工程

Opto-Electronic Engineering

中文核心期刊 中国科技核心期刊
Scopus CSCD

基于保偏光纤与少模光纤的激光温度传感器

陈志萌, 黄昌清

引用本文:

陈志萌, 黄昌清. 基于保偏光纤与少模光纤的激光温度传感器[J]. *光电工程*, 2024, **51**(11): 240185.

Chen Z M, Huang C Q. Laser temperature sensor based on polarization maintaining fiber and few mode fiber[J]. *Opto-Electron Eng*, 2024, **51**(11): 240185.

<https://doi.org/10.12086/oe.2024.240185>

收稿日期: 2024-08-10; 修改日期: 2024-10-25; 录用日期: 2024-10-25

相关论文

基于参考滤波器及互相关算法的碲化镱光纤温度解调方法

毕扬, 熊治富, 李佳文, 杨天宇, 刘兔兔, 万慧明, 董玉明

光电工程 2024, **51**(9): 240143 doi: [10.12086/oe.2024.240143](https://doi.org/10.12086/oe.2024.240143)

一种光纤陀螺全温启动漂移补偿方法

姚磊善, 周一览, 赵帅, 黄腾超, 车双良

光电工程 2024, **51**(5): 240033 doi: [10.12086/oe.2024.240033](https://doi.org/10.12086/oe.2024.240033)

Adaptive decentralized AI scheme for signal recognition of distributed sensor systems

Shixiong Zhang, Hao Li, Cunzheng Fan, Zhichao Zeng, Chao Xiong, Jie Wu, Zhijun Yan, Deming Liu, Qizhen Sun

Opto-Electronic Advances 2024, **7**(12): 240119 doi: [10.29026/oea.2024.240119](https://doi.org/10.29026/oea.2024.240119)

Specialty optical fibers for advanced sensing applications

Huanhuan Liu, Dora Juan Juan Hu, Qizhen Sun, Lei Wei, Kaiwei Li, Changrui Liao, Bozhe Li, Cong Zhao, Xinyong Dong, Yuhan Tang, Yihong Xiao, Gerd Keiser, Perry Ping Shum

Opto-Electronic Science 2023, **2**(2): 220025 doi: [10.29026/oes.2023.220025](https://doi.org/10.29026/oes.2023.220025)

更多相关论文见光电期刊集群网站 



<http://cn.ojournal.org/oe>



OE_Journal



Website

DOI: 10.12086/oe.2024.240185

CSTR: 32245.14.oe.2024.240185

基于保偏光纤与少模光纤的 激光温度传感器

陈志萌, 黄昌清*

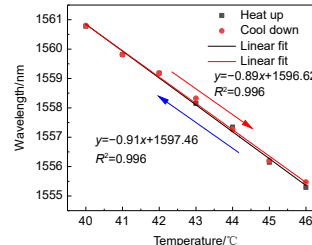
中国计量大学光学与电子科技学院, 浙江 杭州 310018

摘要: 本文提出了一种基于保偏光纤与少模光纤的激光温度传感器, 并对其进行了实验研究。将 20 cm 的保偏光纤与 10 cm 的少模光纤熔接在一起, 之后与 3 dB 耦合器组成 Sagnac 环, 作为传感探头。光经过少模光纤激发出高阶模, 由于少模光纤与保偏光纤直径不匹配, 高阶模与纤芯模耦合到保偏光纤的应力区, 激发出包层模, 从而提高温度灵敏度。实验结果表明, 加入少模光纤后, 传感器的温度灵敏度从 -0.51 nm/°C 提高到 -0.91 nm/°C。该传感器具有精度高、制造方便、本质安全等优点, 在工程结构安全监测中具有广阔的应用前景。

关键词: 少模光纤; 保偏光纤; 光纤萨格纳克干涉仪; 光纤温度传感器; 光纤激光传感器

中图分类号: TN253

文献标志码: A



陈志萌, 黄昌清. 基于保偏光纤与少模光纤的激光温度传感器[J]. 光电工程, 2024, 51(11): 240185

Chen Z M, Huang C Q. Laser temperature sensor based on polarization maintaining fiber and few mode fiber[J]. *Opto-Electron Eng*, 2024, 51(11): 240185

Laser temperature sensor based on polarization maintaining fiber and few mode fiber

Chen Zhimeng, Huang Changqing*

College of Optical and Electronic Technology, China Jiliang University, Hangzhou, Zhejiang 310018, China

Abstract: This paper proposes a laser temperature sensor based on polarization maintaining fiber (PMF) and few-mode fiber (FMF), and conducted their experimental studies. A 20 cm polarization maintaining fiber was spliced with a 10 cm few-mode fiber and then combined with a 3 dB coupler to form a Sagnac loop, which served as the sensing probe. Light passing through the FMF excites higher-order modes. Due to the diameter mismatch between the FMF and PMF, the higher-order modes are coupled into the stress region of the PMF, exciting the cladding modes and thus improving temperature sensitivity. Experimental results show that after adding the FMF, the temperature sensitivity of the sensor increased from -0.51 nm/°C to -0.91 nm/°C. This sensor has the advantages of high precision, easy fabrication, and intrinsic safety, making it highly promising for engineering structure safety monitoring applications.

Keywords: few mode fiber; polarization maintaining fiber; fiber optic Sagnac interferometer; fiber optic temperature sensor; fiber optic laser sensor

收稿日期: 2024-08-10; 修回日期: 2024-10-25; 录用日期: 2024-10-25

基金项目: 浙江省基础公益研究计划 (LGG19A040001)

*通信作者: 黄昌清, cqhuang@cju.edu.cn。

版权所有©2024 中国科学院光电技术研究所

1 引言

近年来, 光纤传感器^[1-4]以其对电磁干扰的高抗扰性、在恶劣环境下的高耐久性和高灵敏度等优点而闻名。鉴于此, 人们将其应用于各种参数的监测, 如折射率^[5-6]、湿度^[7-8]、应变^[9-10]、温度^[11-12]等。在光纤传感器的发展过程中, 人们提出了多种传感结构。这些传感结构包括光纤布拉格光栅^[13-14] (fiber Bragg grating, FBG)、马赫-曾德尔干涉仪^[15-16] (Mach-Zehnder interferometer, MZI)、光纤萨格纳克干涉仪^[17-18] (fiber Sagnac interferometer, FSI)、迈克尔逊干涉仪^[19-20] (Michelson interferometer, MI) 和法布里-珀罗干涉仪^[21-22] (Fabry-Perot interferometer, FPI)。

同时由于光纤激光传感器具有灵敏度高、稳定性好、插入损耗小、信噪比高等优点, 近年来受到越来越多的关注。总的来说, 光纤激光传感器可分为三种类型: 分布式布拉格反射器光纤激光器^[23] (distributed Bragg reflector fiber laser, DBR)、分布式反馈激光器^[24] (distributed feedback laser, DFB) 和光纤环形激光器^[25] (fiber ring laser, FRL)。FRL 由于其谱线适应电信波长窗口, 是良好的温度传感器件。

由于 FRL 凭借其优点被广泛应用于温度传感领域, 并与光纤传感器紧密相连。如 2014 年, Liang 等^[26]提出一种基于锥形无包层单模光纤结构的全光纤环形传感器, 锥形无包层单模光纤结构同时作为激光系统的传感器和滤波器, 在 8~80 °C 的温度范围内, 传感器的灵敏度达到 10.8 pm/°C。2021 年, Lin 等^[27]提出一种基于掺铒上锥和花生状光纤结构的光纤环形激光器, 花生状结构结合上锥形结构可以有效地激发包层模, 从而在掺铒光纤复合结构中获得清晰的干涉图样, 传感器的温度灵敏度为 301 pm/°C。2022 年, Sanchez-Gonzalez 等^[28]提出一种由人工背散射反射器辅助的双波长 C 波段掺铒光纤激光器, 这种基于光纤的反射器是通过飞秒激光直写技术刻入单模光纤中的, 在 35~75 °C 的温度范围内, 传感器的灵敏度达到了 9.29 pm/°C。2022 年, Lin 等^[29]提出一种基于光纤环形腔中上锥光纤结构的掺铒光纤马赫-曾德尔干涉仪, 该结构能够同时充当滤波器、传感器和增益介质。由于掺铒光纤具有较高的热光系数, 在 10~50 °C 范围内, 传感器的灵敏度达到 0.261 nm/°C。2024 年, Liu 等^[30]提出一种基于碳纳米管包覆的锥形保偏光纤

的光纤环形激光器, 同时使用聚甲基丙烯酸甲酯进行封装, 聚甲基丙烯酸甲酯的膨胀使得传感结构对热变化敏感, 传感器的灵敏度达到 0.77 nm/°C。

本文提出了一种基于保偏光纤 (polarization maintaining fiber, PMF) 和少模光纤 (few mode fiber, FMF) 的 Sagnac 环光纤激光温度传感器, 由一段 PMF 和一段 FMF 熔接相连, 之后与 3 dB 四端口耦合器组成 FMF-PMF 的 Sagnac 环, 作为温度传感器。由于纤芯不匹配, 激发出高阶模, 高阶模和纤芯模耦合到 PMF 的应力区, 转变为包层模, 提高了温度灵敏度。实验结果表明, PMF-Sagnac 环光纤激光温度传感器的温度灵敏度为 -0.57 nm/°C; 而加入 FMF 后, 基于 FMF-PMF 的 Sagnac 环光纤激光温度传感器的温度灵敏度为 -0.91 nm/°C, 提高了 1.6 倍。

2 基于 FMF-PMF 的 Sagnac 环制作与工作原理

基于 FMF-PMF 的 Sagnac 环结构如图 1 所示, 由 20 cm 的 PMF 和 10 cm 的 FMF 熔接在一起, 通过法兰盘将其与 3 dB 四端口耦合器连接形成 Sagnac 环, 作为传感器。其中 PMF (PM15-17034) 是熊猫型光纤, FMF 是四模光纤 (阶跃型), 纤芯直径为 18.5 μm。输入光经过 3 dB 四端口耦合器分成两束光, 一束光顺时针传输, 其先经过 FMF, 由于纤芯不匹配, 激发出高阶模, 高阶模和纤芯模耦合到 PMF 的应力区, 转变为包层模, 之后纤芯模与包层模耦合到 SMF 纤芯中; 而另一束光逆时针传输, 其先经过 PMF, 然后由于 FMF 和 PMF 纤芯不匹配, 激发出高阶模, 之后高阶模与纤芯模耦合到 SMF 纤芯中, 最后在 3 dB 耦合器中耦合形成干涉。

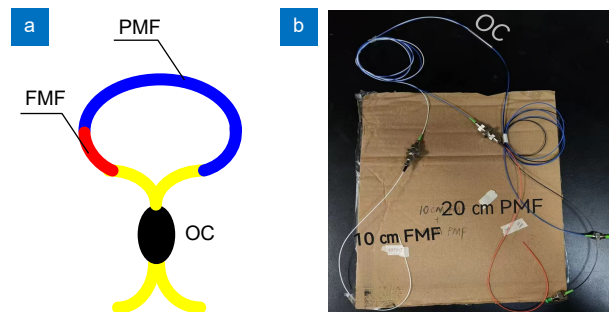


图 1 基于 FMF-PMF 的 Sagnac 环传感器。

(a) 结构示意图; (b) 实物图

Fig. 1 Sagnac ring sensor based on the FMF-PMF.

(a) Schematic diagram of the structure; (b) A physical image of the sensor

在理想条件下, 忽略熔接过程中产生的损耗以及光纤和耦合器的耦合熔堆区的偏振效应。基于 FMF-PMF 的 Sagnac 环的传输频谱近似为一个周期波长相关函数, 其传输函数可以表示为^[31]

$$T_{\text{FMF-PMF}} = \frac{1 - \cos \varphi}{2}, \quad (1)$$

$$\varphi = \frac{2\pi(\Delta n L_1 + \Delta n_{\text{eff}} L_2)}{\lambda}, \quad (2)$$

其中: φ 是基于 FMF-PMF 的 Sagnac 环的相位差, Δn 是 PMF 的快轴和慢轴的双折射率差, Δn_{eff} 是纤芯模和高阶模之间的有效折射率之差, L_1 是 PMF 的长度, L_2 是 FMF 的长度, λ 是入射光波的波长。

当 $\varphi = 2m\pi$ ($m=0, 1, 2, 3, \dots$, λ_m 是 m 阶波谷对应的波长) 时, 透射谱函数将达到最小值, 在波形上出现波谷。FSR 的定义为两个相邻波谷之间的间隔, 可表示为

$$\begin{aligned} \text{FSR}_{\text{FMF-PMF}} &= \lambda_m - \lambda_{m+1} = \frac{\lambda_m \lambda_{m+1}}{\Delta n L_1 + \Delta n_{\text{eff}} L_2} \\ &\approx \frac{\lambda_m^2}{\Delta n L_1 + \Delta n_{\text{eff}} L_2}. \end{aligned} \quad (3)$$

忽略基于 FMF-PMF 的 Sagnac 环光纤结构长度

变化的温度诱导波长变化可以表示为

$$\Delta \lambda = \frac{\lambda}{\Delta n L_1 + \Delta n_{\text{eff}} L_2} \left(\frac{\partial \Delta n}{\partial T} L_1 + \frac{\partial \Delta n_{\text{eff}}}{\partial T} L_2 \right) \Delta T, \quad (4)$$

其中: ΔT 是温度变化量。由式 (4) 可知, 基于 FMF-PMF 的 Sagnac 环的温度灵敏度与 FMF 有关。

为了研究不同长度的 FMF 对 FMF-PMF 的 Sagnac 环的输出光谱, 制作 PMF 的长度为 20 cm, FMF 的长度分别为 0 cm、5 cm、10 cm、15 cm 的传感器。在光源为宽带光源时, 该传感器的输出光谱如图 2 所示。

由图 2 可知, 当 FMF 的长度为 15 cm 时, 该传感器的输出光谱有杂波, 故选取 FMF 的长度为 10 cm。

3 实验结果与分析

本文基于 FMF-PMF 的 Sagnac 环光纤环形激光传感器的实验装置示意图如图 3 所示, 基于 FMF-PMF 的 Sagnac 环光纤激光温度传感器采用环形腔结构形式, 由 980 nm 泵浦激光器 (输出光功率 0~521 mW)、980/1550 nm 波分复用器 (wavelength division

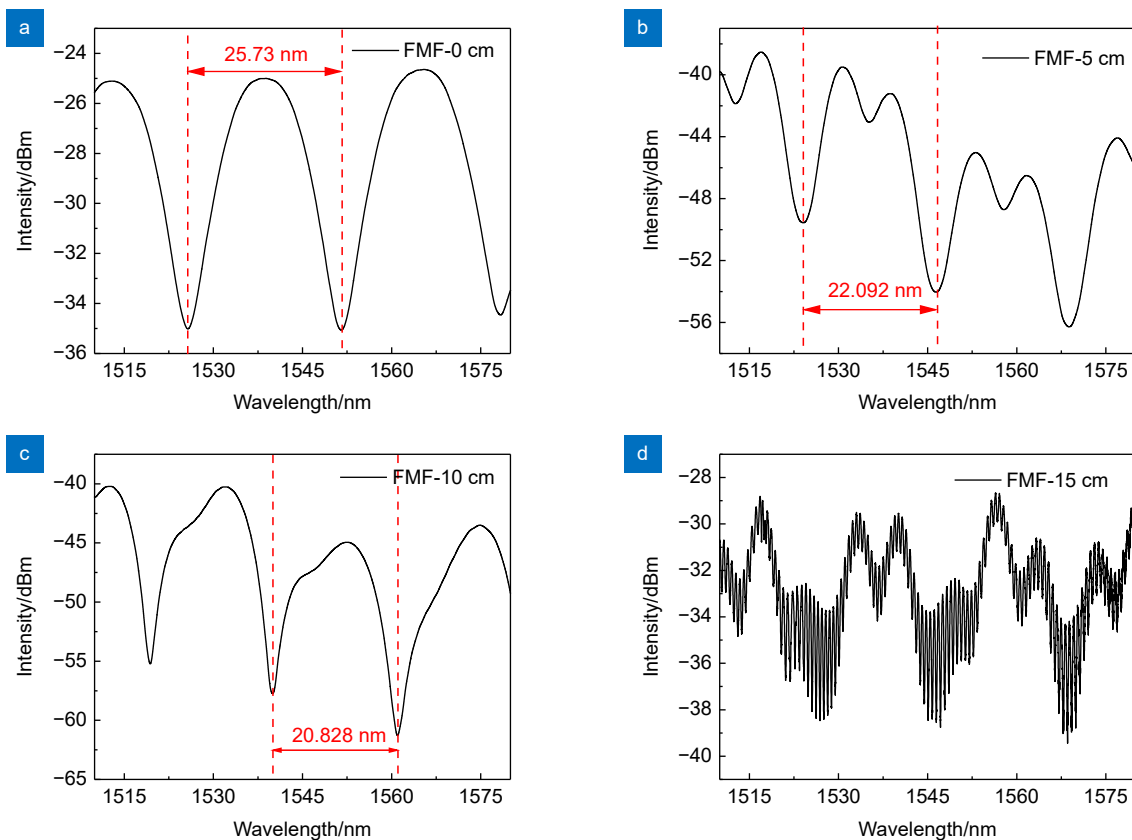


图 2 当 PMF=20 cm 时, 不同长度 FMF 的输出光谱。(a) FMF=0 cm; (b) FMF=5 cm; (c) FMF=10 cm; (d) FMF=15 cm
Fig. 2 When PMF is 20 cm, the output spectra for different lengths of FMF. (a) FMF=0 cm; (b) FMF=5 cm; (c) FMF=10 cm; (d) FMF=15 cm

基于 FMF-PMF 的 Sagnac 环光纤结构固定在加热台上, 泵浦功率选取为 175 mW, 加热台从 40 °C 加热到 46 °C, 每隔 1 °C, 等待 10 分钟加热台板温度稳定后, 保存下输出光谱, 如图 8 所示。在实验开始后, 一定要避免触碰基于 FMF-PMF 的 Sagnac 环传感探头, 以保证测量结果的准确性, 其输出光谱如图 8 所示。

由图 8(a) 可知, 单峰波长会随着温度的升高, 向短波长方向移动 (蓝移)。这是因为温度升高时, PMF 的纤芯模与包层模的双折射率差和 FMF 的基模与高阶模的有效折射率之差减小引起的。为了测量其稳定性, 进行了温度下降实验, 实验结果如图 8(b) 所示, 随着温度的下降, 单峰波长会进行红移, 也就是向长波长方向移动。这是因为温度下降时, PMF 的纤芯模与包层模的双折射率差和 FMF 的基模与高阶模的有效折射率之差增大引起的。

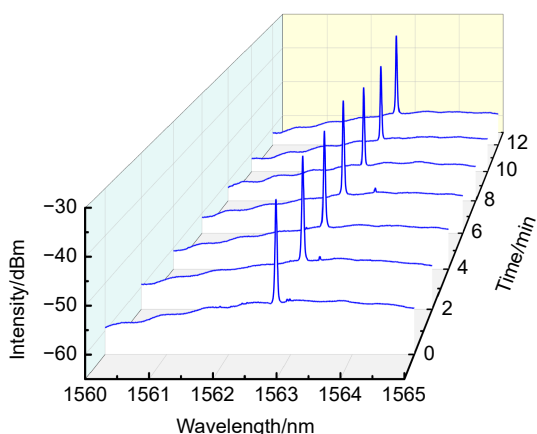


图 6 在 175 mW 泵浦功率下每隔 2 min 记录的激光输出光谱
Fig. 6 Laser output spectra intensities recorded at 2 min intervals under 175 mW pump power

如图 9 所示, 通过追踪单峰波长, 绘制了升温 and 降温时单峰波长与温度变化的关系曲线, 使用线性拟合后, 得到升温时的温度灵敏度和线性拟合度, 分别为 -0.91 nm/°C 和 0.996; 降温时的温度灵敏度和线性拟合度分别为 -0.89 nm/°C 和 0.996, 具有较好的线性关系。同时, 观察到升温 and 降温的过程中, 在相同温度时, 单峰波长的数值几乎一致, 体现出良好的稳定性。

为了研究 FMF-PMF 的 Sagnac 环的温度灵敏度与 FMF 的关系, 制作并搭建了长度为 20 cm 的 PMF-Sagnac 环光纤激光温度传感器, 进行实验。实验过程与之前相同, PMF-Sagnac 环光纤结构固定在加热台上, 泵浦功率选取为 175 mW, 加热台从 40 °C 加热到 46 °C, 每隔 1 °C, 等待 10 min 加热台板温度稳定后, 保存下输出光谱, 如图 10 所示。

由图 10(a) 可知, 单峰波长会随着温度的升高进

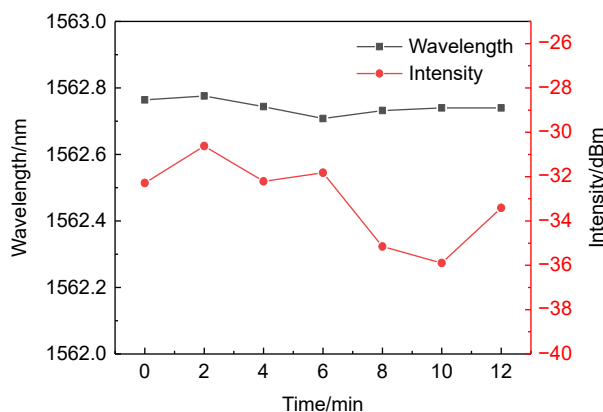


图 7 不同时间下输出峰的中心波长和峰值强度
Fig. 7 Center wavelengths and peak intensity of output peaks at different times

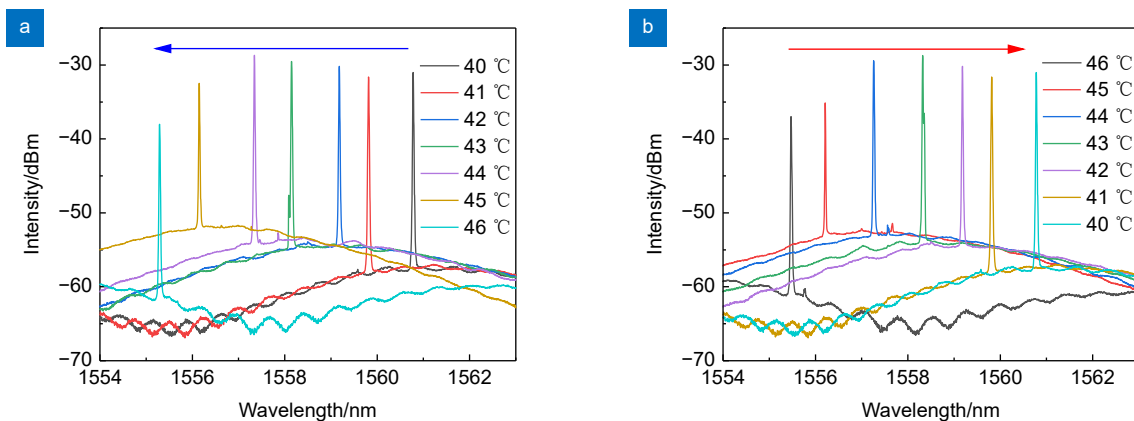


图 8 不同温度下基于 FMF-PMF 的 Sagnac 环光纤激光温度传感器的输出光谱。(a) 升温; (b) 降温

Fig. 8 Output spectra of FMF-PMF based Sagnac ring fiber laser temperature sensors at different temperatures. (a) Heat up; (b) Cool down

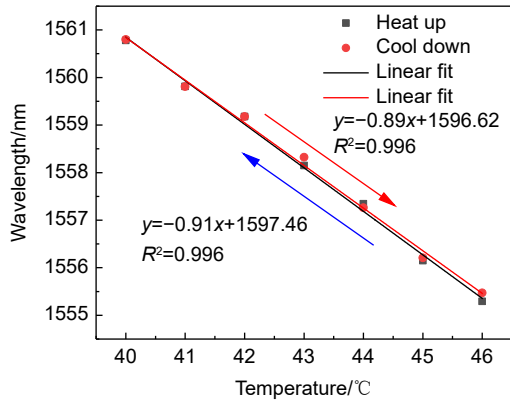


图 9 基于 FMF-PMF 的 Sagnac 环的温度与波长的关系曲线

Fig. 9 Relationship curve between temperature and wavelength of FMF-PMF based Sagnac rings

行蓝移, 也就是向短波长方向移动。这是因为温度升高时, PMF 的快轴和慢轴的双折射率之差变小导致的。为了测量其稳定性, 进行了温度下降实验, 实验

结果如图 10(b) 所示。随着温度的下降, 单峰波长会进行红移, 也就是向长波长方向移动。这是因为温度升高时, PMF 的快轴和慢轴的双折射率之差变大。

如图 11 所示, 通过追踪单峰波长, 绘制了升温 and 降温时单峰波长与温度变化的关系曲线, 使用线性拟合后, 得到升温时的温度灵敏度和线性拟合度, 分别为 $-0.57 \text{ nm}/^\circ\text{C}$ 和 0.999; 降温时的温度灵敏度和线性拟合度分别为 $-0.57 \text{ nm}/^\circ\text{C}$ 和 0.999, 具有较好的线性关系。同时, 观察到升温 and 降温的过程中, 在相同温度时, 单峰波长的数值几乎一致, 这体现出良好的稳定性。

为了体现出该传感器的高灵敏特性, 与其他的光纤温度传感器进行比较, 如表 1 所示。由表可知, 本文的光纤温度传感器的温度灵敏度比其他光纤温度传感器的温度灵敏度有着明显的提高。这说明在 PMF-sagnac 中加入 FMF 能够有效的提高温度灵敏度。

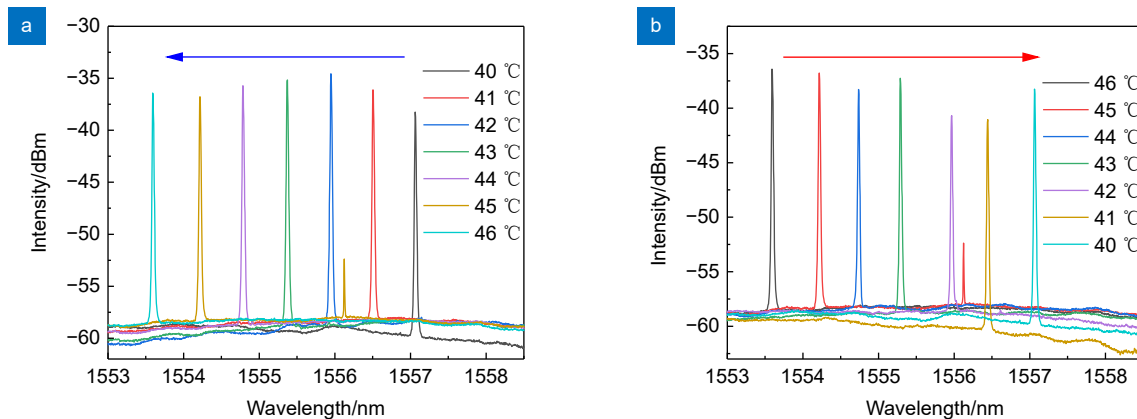


图 10 不同温度下基于 PMF 的 Sagnac 环光纤激光温度传感器的输出光谱。(a) 升温; (b) 降温

Fig. 10 Output spectra of PMF-based Sagnac ring fiber laser temperature sensors at different temperatures. (a) Heat up; (b) Cool down

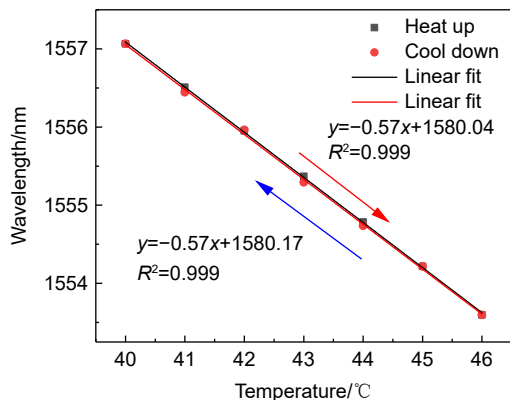


图 11 基于 PMF 的 Sagnac 环的温度与波长的关系曲线

Fig. 11 Relationship curve between temperatures and wavelengths of PMF based Sagnac rings

表 1 与先前报道文献的传感器性能对比分析

Table 1 Performance analysis of the proposed probe with that reported in literature

| 年份 | 类别 | 温度灵敏度 | 参考文献 |
|------|-----------------------------|-------------|------|
| 2014 | 基于锥形无包层单模光纤结构的全光纤环形传感器 | 10.8 pm/°C | [26] |
| 2021 | 基于掺铒上锥和花生状光纤结构的光纤环形激光器 | 301 pm/°C | [27] |
| 2022 | 基于人工背散射反射器辅助的双波长C波段掺铒光纤激光器 | 9.29 pm/°C | [28] |
| 2022 | 基于光纤环形腔中上锥光纤结构的掺铒光纤马赫曾德尔干涉仪 | 0.261 nm/°C | [29] |
| 2024 | 基于碳纳米管包覆的锥形保偏光纤的光纤环形激光器 | 0.77 nm/°C | [30] |
| 2024 | 基于FMF-PMF的Sagnac环光纤激光温度传感器 | 0.91 nm/°C | 本文 |

4 结论

本文提出了一种基于 FMF-PMF 的 Sagnac 环光纤激光温度传感器, 其中一段长为 20 cm 的保偏光纤和一段长为 10 cm 的少模光纤熔接相连, 之后与 3 dB 四端口耦合器组成 FMF-PMF 的 Sagnac 环, 作为温度传感器。实验结果表明, PMF-Sagnac 环光纤激光温度传感器的温度灵敏度为 $-0.57 \text{ nm}/^\circ\text{C}$, 且具有 0.999 的线性拟合度。而加入 FMF 后, 基于 FMF-PMF 的 Sagnac 环光纤激光温度传感器的温度灵敏度为 $-0.91 \text{ nm}/^\circ\text{C}$, 且具有 0.996 的线性拟合度, 灵敏度提高了 1.6 倍。该光纤激光温度传感器具有成本较低、易制作、灵敏度高的优点, 适用于对温度变化监测要求较高的设备。

参考文献

- [1] Liu Y X, Li X G, Zhang Y N, et al. Fiber-optic sensors based on Vernier effect[J]. *Measurement*, 2021, **167**: 108451.
- [2] Wu T G, Liu G W, Fu S G, et al. Recent progress of fiber-optic sensors for the structural health monitoring of civil infrastructure[J]. *Sensors*, 2020, **20**(16): 4517.
- [3] Fan L, Bao Y. Review of fiber optic sensors for corrosion monitoring in reinforced concrete[J]. *Cem Concr Compos*, 2021, **120**: 104029.
- [4] Zheng Y, Zhu Z W, Xiao W, et al. Review of fiber optic sensors in geotechnical health monitoring[J]. *Opt Fiber Technol*, 2020, **54**: 102127.
- [5] Lei X Q, Dong X P, Sun T, et al. Ultrasensitive refractive index sensor based on Mach-Zehnder interferometer and a $40\mu\text{m}$ fiber[J]. *J Lightwave Technol*, 2021, **39**(17): 5625–5633.
- [6] Gao Z G, Feng Y H, Chen H L, et al. Refractive index and temperature sensing system with high sensitivity and large measurement range using an optical fiber[J]. *IEEE Trans Instrum Meas*, 2023, **72**: 9502706.
- [7] Zhao L, Wang J Q, Li Z, et al. Quasi-distributed fiber optic temperature and humidity sensor system for monitoring of grain storage in granaries[J]. *IEEE Sens J*, 2020, **20**(16): 9226–9233.
- [8] Qin Z G, Qu S, Wang Z Q, et al. A fully distributed fiber optic sensor for simultaneous relative humidity and temperature measurement with polyimide-coated polarization maintaining fiber[J]. *Sens Actuators B Chem*, 2022, **373**: 132699.
- [9] Fedorov A Y, Kosheleva N A, Matveenko V P, et al. Strain measurement and stress analysis in the vicinity of a fiber Bragg grating sensor embedded in a composite material[J]. *Compos Struct*, 2020, **239**: 111844.
- [10] Dong L G, Gang T T, Bian C, et al. A high sensitivity optical fiber strain sensor based on hollow core tapering[J]. *Opt Fiber Technol*, 2020, **56**: 102179.
- [11] Cui Y, Jiang Y, Liu T M, et al. A dual-cavity Fabry-Perot interferometric fiber-optic sensor for the simultaneous measurement of high-temperature and high-gas-pressure[J]. *IEEE Access*, 2020, **8**: 80582–80587.
- [12] Lu J Y, Yu Y, Qin S P, et al. High-performance temperature and pressure dual-parameter sensor based on a polymer-coated tapered optical fiber[J]. *Opt Express*, 2022, **30**(6): 9714–9726.
- [13] Liu Y G, Feng Y P, Wen J L, et al. Integrated fiber-optic sensor based on inscription of FBG in seven-core fiber for curvature and temperature measurements[J]. *Opt Fiber Technol*, 2023, **75**: 103197.
- [14] Braunfelds J, Senkans U, Skels P, et al. FBG-based sensing for structural health monitoring of road infrastructure[J]. *J Sens*, 2021, **2021**(1): 8850368.
- [15] Wang Y, Tong R J, Zhao K J, et al. Optical fiber sensor based on SPR and MZI for seawater salinity and temperature measurement[J]. *Opt Laser Technol*, 2023, **162**: 109315.
- [16] Gao S, Ji C K, Ning Q Y, et al. High-sensitive Mach-Zehnder interferometric temperature fiber-optic sensor based on core-offset splicing technique[J]. *Opt Fiber Technol*, 2020, **56**: 102202.
- [17] Liu S T, Zhao S X, Liu Q W, et al. Ultrahigh-resolution and ultra-simple fiber-optic sensor with resonant Sagnac interferometer[J]. *Opt Lett*, 2023, **48**(13): 3543–3546.
- [18] Ge Q, Zhu J H, Cui Y Y, et al. Fiber optic temperature sensor utilizing thin PMF based Sagnac loop[J]. *Opt Commun*, 2022, **502**: 127417.
- [19] Guo J H, Lian S P, Zhang Y, et al. High-temperature measurement of a fiber probe sensor based on the Michelson interferometer[J]. *Sensors*, 2021, **22**(1): 289.
- [20] Shao M, Zhang R, Zhao X, et al. Dual-core fiber based in-line Michelson interferometer for humidity sensing[J]. *Opt Fiber Technol*, 2021, **64**: 102570.
- [21] Liu Y G, Wen J L, Feng Y P, et al. Miniaturized high-sensitivity temperature sensor based on cascaded fiber-optic FPI[J]. *IEEE Photonics Technol Lett*, 2023, **35**(8): 430–433.
- [22] Liang J Q, Yu Y, Bian Q, et al. Metal-coated high-temperature strain optical fiber sensor based on cascaded air-bubble FPI-FBG structure[J]. *Opt Express*, 2023, **31**(10): 16795–16811.
- [23] Liu B, Zhang H. Polarimetric distributed Bragg reflector fiber laser sensor array for simultaneous measurement of transverse load and temperature[J]. *Opt Fiber Technol*, 2011, **17**(6): 619–625.
- [24] Han S X, Yan J Y, Cao C F, et al. Single-mode GaSb-based laterally coupled distributed-feedback laser for CO_2 gas detection[J]. *Chin Phys B*, 2023, **32**(10): 104205.
- [25] Feng D Q, Tang Y X, Lei R, et al. A Polarimetric fiber ring laser incorporating a coupled optoelectronic oscillator and its application to magnetic field sensing[J]. *Photonics*, 2023, **10**(6): 662.
- [26] Liang L J, Ren G B, Yin B, et al. Refractive index and temperature sensor based on fiber ring laser with STCS fiber structure[J]. *IEEE Photonics Technol Lett*, 2014, **26**(21): 2201–2204.
- [27] Lin W H, Zhou S J, Shao L Y, et al. In-fiber Mach-Zehnder interferometer based on Er doped up-taper and peanut-shaped fiber structure in fiber ring laser[J]. *IEEE Access*, 2021, **9**: 128126–128132.
- [28] Sanchez-Gonzalez A, Perez-Herrera R A, Roldan-Varona P, et al. A dual-wavelength fiber laser sensor with temperature and strain discrimination[J]. *Sensors*, 2022, **22**(18): 6888.
- [29] Lin W H, Liu Y H, Shum P P, et al. In-line Mach Zehnder

interferometer based on ytterbium doped fiber with up-taper structure in fiber ring laser and its application in sensing[J]. *Sensors*, 2022, 22(23): 9196.

- [30] Liu B W, Shirahata T, Ye G Y, et al. Hybrid wavelength manipulation with enhanced ambient-thermal adaptability in an all-polarization-maintaining mode-locked fiber laser[J]. *J*

Lightwave Technol, 2024, 42(9): 3376–3384.

- [31] Chen Z M, Huang C Q, Zhu Q C, et al. Temperature sensor of cascaded sagnac interferometer based on vernier effect[J]. *Semicond Optoelectron*, 2023, 44(6): 845–850.

陈志萌, 黄昌清, 朱庆超, 等. 基于游标效应的萨格纳克干涉仪温度传感器[J]. *半导体光电*, 2023, 44(6): 845–850.

作者简介



陈志萌 (1998-), 男, 硕士研究生, 主要研究方向为光纤温度传感技术。

E-mail: 2368678239@qq.com



【通信作者】黄昌清 (1980-), 男, 博士, 主要研究方向为光纤激光器和传感器、光子晶体光纤的研究。

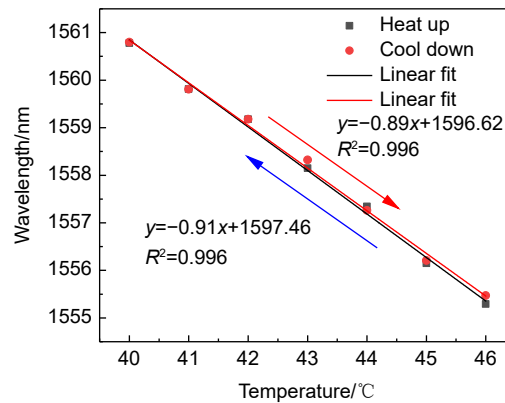
E-mail: cqhuang@cjlu.edu.cn



扫描二维码, 获取PDF全文

Laser temperature sensor based on polarization maintaining fiber and few mode fiber

Chen Zhimeng, Huang Changqing*



Relationship curve between temperature and wavelength of FMF-PMF based Sagnac rings

Overview: As we all know, temperature has always been an important parameter in physics, and various tools have been used to measure temperature. In recent decades, fiber optic interferometers have been widely used in temperature measurement. Traditional fiber optic interferometers include the Mach-Zehnder interferometer (MZI), Fabry-Perot interferometer (FPI), Michelson interferometer (MI), and fiber optic Sagnac interferometer (FSI). Meanwhile, fiber optic ring lasers have advantages such as high sensitivity, good stability, low insertion loss, and high signal-to-noise ratio, leading to the combination of fiber optic interferometers with fiber optic ring lasers. Among these, the FSI has advantages of low noise, reciprocal dual optical paths, and higher temperature sensitivity compared to MZI and FPI, thus being widely used in temperature measurement.

This paper proposes a laser temperature sensor based on polarization-maintaining fiber (PMF) and few-mode fiber (FMF) and conducts experimental research on its sensing characteristics. A 20 cm PMF is spliced with a 10 cm FMF, then combined with a 3 dB coupler to form an FMF-PMF Sagnac ring as a temperature sensor. Light passing through the FMF excites higher-order modes, and due to the diameter mismatch between the FMF and PMF, the higher-order modes and core modes couple into the stress region of the PMF, exciting cladding modes and thereby enhancing temperature sensitivity. In the temperature sensitivity measurement experiment of the FMF-PMF Sagnac ring, the temperature range from 40 °C to 46 °C with a step size of 1 °C, maintaining each temperature for about 10 minutes, after which the output spectrum is recorded by a spectrum analyzer. Experimental results show that as the temperature increases, the single peak wavelength shifts to shorter wavelengths (blue shift), caused by the reduction in the birefringence difference between the PMF core mode and cladding mode and the effective refractive index difference between the FMF fundamental mode and higher-order mode, with a temperature sensitivity of -0.91 nm/°C and a fitting curve fit degree of 0.996. As the temperature decreases, the single peak wavelength shifts to longer wavelengths (red shift), caused by the increase in the birefringence difference between the PMF core mode and cladding mode. At the same time, the effective refractive indexes are different between the FMF fundamental mode and higher-order mode, with a temperature sensitivity of -0.89 nm/°C and a fitting value of 0.996. The temperature sensitivity of the PMF-Sagnac ring fiber laser temperature sensor is -0.57 nm/°C. Thus, it can be seen that with the addition of FMF, the temperature sensitivity of the FMF-PMF Sagnac ring fiber laser temperature sensor is increased by 1.6 times.

Chen Z M, Huang C Q. Laser temperature sensor based on polarization maintaining fiber and few mode fiber[J]. *Opto-Electron Eng*, 2024, 51(11): 240185; DOI: [10.12086/oe.2024.240185](https://doi.org/10.12086/oe.2024.240185)

Foundation item: Project supported by Basic Public Welfare Research Program of Zhejiang Province (LGG19A040001)
College of Optical and Electronic Technology, China Jiliang University, Hangzhou, Zhejiang 310018, China

* E-mail: cqhuang@cju.edu.cn